TOP-CT: Trajectory with Overlapping Projections X-ray Computed Tomography

Dirk Elias Schut, Kees Joost Batenburg, Robert van Liere, Tristan van Leeuwen

Abstract—TOP-CT (Trajectory with Overlapping Projections X-ray Computed Tomography) is a new class of CT scanning geometries for high throughput industrial CT scanning. In TOP-CT multiple objects move with a constant spacing over the same trajectory between a stationary X-ray source and detector. The projections of multiple objects can overlap, which provides additional flexibility when designing CT scanning geometries. Reconstruction algorithms were developed to reconstruct objects one by one from the overlapping projection data as soon as the objects move out of the field of view of the scanning setup. This makes it possible to make reconstructions while new objects with overlapping projections keep being added.

The forward problem of TOP-CT is linear with a band block Toeplitz structure, and the matrix of the forward problem can be constructed from multiple copies of a non-overlapping CT projection matrix, so existing software toolkits can be used for TOP-CT with only a small modification. Simulation experiments and a real life experiment were performed on a U-turn TOP-CT geometry. One experiment showed that reconstructions from an overlapping projection setup have a slightly higher SSIM (0.828 vs 0.811) and similar PSNR (33.50 vs 33.34) compared to a non-overlapping setup, using the same scan time per object and the same reconstruction algorithm (SIRT). Another experiment showed that a reconstruction algorithm making reconstructions one by one using only local projection data performed without loss of quality compared to a baseline reconstruction method using all projection data.

Index Terms—computed tomography (CT), CT scanning geometry, overlapping X-ray projections, non destructive testing (NDT), iterative methods, block Toeplitz matrix

Fig. 1. Comparison of different X-ray tomography geometries. For every geometry an illustration of the geometry is given on the left and an example of a projection image obtained from the geometry is given on the right. Top: Standard circular cone beam geometry with a rotating object, Middle: Rotation and translation geometry, where objects rotate while they move over a line. Bottom: One example of the class of geometries presented in this paper.

I. INTRODUCTION

X-RAY computed tomography (CT) is widely used in industry to inspect the inside of objects in 3D without destroying them [3, 20, 24]. In the context of smart factories and industry 4.0, CT could also be used for quality control in factories by scanning every product after production [1]. To meet the high throughput demands of factory applications, CT scanners need to have a short acquisition time per object.

In a CT scanner a series of 2D X-ray projection images are acquired from multiple directions, and these images are combined to reconstruct a 3D representation of the inside of the object. The way in which the object, the X-ray source and the detector move relative to each other is called the geometry of a scanner. To achieve a good reconstruction quality over the entire object it is important that there is enough variation in the directions from which the projection images are acquired. This is formalized in a completeness condition by Tuy [25]

and Smith [23]. However, some geometries do not meet the completeness condition but still obtain acceptable results in practice [6, 18]. To distinguish these slightly incomplete scanning geometries, measures have been derived that provide a completeness indication between zero and one over the space of an object [13, 15].

A CT scanner on a production line should have a geometry that is sufficiently complete to be able to perform the desired inspection tasks while also having a low acquisition time per object. For the application of scanning logs in a sawing plant a CT scanner is commercially available where the logs move through a rotating gantry [26, 7, 8]. The X-ray source and detector are attached to the gantry which is rotating at high speed to quickly obtain images from different angles. A similar setup is used in medical CT scanners. Another high-throughput scanner is commercially available for the application of explosives detection in luggage [16]. Instead of a rotating gantry it uses multiple multi-focus sources and detectors in a ring around the conveyor belt, making it possible to acquire similar data to a rotating gantry with a stationary

setup.

Depending on the type of object, applying additional movement to the object while the source and detector are stationary, can be a simpler alternative to acquire a sufficiently complete set of projection data. In the rotation and translation geometry [4] each object moves in a straight line parallel to a large flat panel detector while each object also rotates around its vertical axis. Further research on this geometry has improved the computation time [12]. Moreover, the reconstruction results when using a low number of projections were improved by assuming a limited number of attenuation levels within the object, and by using the outer shape of the object, which could be acquired by other sensors, i.e. optical sensors [19].

The throughput of a rotation and translation geometry is determined by two parameters: the spacing between objects, and the translation speed. The spacing between objects is limited by the fact that projections of two adjacent objects should not overlap. Moreover, if the translation speed is increased, the rotation speed or detector size should also be increased to still acquire a complete set of projection images. Increasing the translation speed or rotation speed has the downside of introducing motion blur and vibrations in the objects, while increasing the detector size increases the cost of the setup.

In this paper a new class of geometries is introduced called TOP-CT (Trajectory with Overlapping Projections X-ray Computed Tomography). In a TOP-CT scanner multiple objects move over the same trajectory between a stationary source and detector, and the projections of multiple objects overlap. By allowing projections to overlap, the spacing between objects can be reduced to zero, which increases the throughput of a scanner. Moreover the trajectory of the objects can be modified so that an object passes the same part of a detector more than once. This makes it possible to reduce the detector size, without changing the throughput, rotation speed, or translation speed. An illustration of what differentiates TOP-CT from existing geometries is given in Figure 1. One way to realize the TOP-CT U-turn geometry from Figure 1 would be to use a hanging overhead conveyor, because in such systems objects rotate with the curve of the conveyor track, just like in the illustration.

Reconstructing objects from overlapping projections has been investigated before [14]. Their method was intended to be used with projection data acquired at a synchrotron beamline, so it assumed a parallel beam source. The objects were placed on a line between the source and detector, and each object was rotated individually. For the reconstruction algorithm to be able to distinguish individual objects, small offsets in position were applied to each object that differ for every projection image acquired. An important difference between TOP-CT and [14] is the way in which new objects are introduced. In [14] objects are scanned in batches, so the projections of objects only overlap within a batch. In TOP-CT new objects are introduced at a constant rate, resulting in overlapping projections between all adjacent objects. While this makes the reconstruction problem more complicated, it simplifies the mechanical setup because objects on a production line can maintain a constant speed while going through the scanner

and it eliminates the time required to replace the batch, during which the detector is not utilized.

The contributions of this paper are as follows: In Section II a mathematical formulation is given for the TOP-CT forward problem. It is shown to be a linear problem, where the matrix has a block-Toeplitz structure, and it can be constructed from multiple copies of the projection matrix of a single object. In Section III four reconstruction methods for TOP-CT are presented. One method uses all projection data similarly to [14], while the other methods only use local projection data, enabling on-line reconstructions. In Section IV the reconstruction quality of the different methods is evaluated experimentally, with the on-line *submatrix* method reaching the same reconstruction quality as the baseline *together* method. Finally a discussion and conclusion are given in Sections V and VI.

II. FORWARD PROBLEM

In this section first the forward problem of CT scanning a single object is reviewed. This formulation is extended to include multiple objects. When all objects move over the same conveyor belt the problem has a block matrix structure which is also investigated.

A. Single object

A CT scanner consists of a source, a detector and some kind of stage or conveyor moving an object. Conventional X-ray scanners rotate the object, or rotate the source and detector around the object, but many scanning geometries are possible.

The source emits high energy photons in the direction of the object. Within the object some of these photons are absorbed or scattered in a different direction, and the other photons are captured by the detector. The detector is a flat panel, consisting of many pixels. At a fixed frequency in time, each pixel measures how many photons have arrived within the pixel area since the previous measurement. By changing the relative positions of the source, detector and object over time many measurements of the inside of the object are collected. According to the Beer-Lambert law each measurement can be represented as the exponent of a line-integral over the line segment from the source to the detector pixel:

$$I_d = I_0 \exp\left(-\int_{\mathbb{R}} x(\boldsymbol{s} + t\boldsymbol{\eta})dt\right). \quad (1)$$

In the above formula I_0 is the number of photons emitted by the source and I_d is the number of photons reaching the detector. $x(\boldsymbol{p})$ is a function representing the attenuation coefficient of the object at position $\boldsymbol{p}$. $\boldsymbol{s}$ and $\boldsymbol{\eta}$ represent the starting position and direction of the photons. For further computations the measurements are preprocessed to make the right hand side of the equation linear:

$$y = -\log\left(\frac{I_d}{I_0}\right) = \int_{\mathbb{R}} x(\boldsymbol{s} + t\boldsymbol{\eta})dt. \quad (2)$$

The domain of the absorption function x can be discretized to obtain a vector $\boldsymbol{x} \in \mathbb{R}^n$ consisting of $n = N_h \times N_v \times N_d$ (horizontal, vertical, depth) voxels. All the preprocessed measurements can be bundled into a vector $\boldsymbol{y} \in \mathbb{R}^m$ consisting

of $m = M_h \times M_v \times M_t$ (horizontal and vertical detector pixels and the number of time steps) measurements. Together they can be used to form a matrix vector equation:

$$y = Ax. \tag{3}$$

In this equation $A \in \mathbb{R}^{m \times n}$ describes how the measurements in y relate to the attenuation coefficients x over the volume. The entries of A are determined by how the object, source and detector move over time.

B. Multiple objects with overlapping projections

When multiple objects are positioned between the source and detector the projections of these objects overlap on the detector. An example of a scanning geometry where this happens is given in Figure 1 (bottom).

If an X-ray first passes through object x_1 and then through object x_2 the line integral for calculating the the intensity of the ray at the detector will also contain both volumes:

$$I_d = I_0 \exp\left(-\int_{\mathbb{R}} x_1(s + t\eta) + x_2(s + t\eta)dt\right). \tag{4}$$

These measurements can be preprocessed in the same way as in equation 2 and all measurements can again be bundled into a vector y_c, where the c stands for *combined* projection data. This makes it possible to formulate the forward problem as a matrix vector equation:

$$A_1 x_1 + A_2 x_2 = y_1 + y_2 = y_c. \tag{5}$$

The sum of two matrix vector products can be described as a single matrix vector product. The geometry matrices A_1 and A_2 can be combined into combined geometry matrix B and volume vectors x_1 and x_2 can be stacked into one combined volume vector x_c:

$$B x_c = A_1 x_1 + A_2 x_2 = y_c. \tag{6}$$

The same principle can also be applied for more than two objects. Streams of any length can be represented in the above form.

C. Noise

The physical processes causing the noise in overlapping projection data are the same as for conventional CT [28]. A common way to model the noise is to assume Poisson noise on the detector measurements before preprocessing I_d [9]. Given a sufficiently high I_d, noise in the projection data can be modelled with an additive noise vector $\epsilon \in \mathbb{R}^m$ with a Gaussian distribution:

$$\overline{y_c} = B x_c + \epsilon. \tag{7}$$

D. Structure of matrix B

When all objects are moving on the same conveyor belt, the only difference between A_1 and A_2 is the starting time of the object. Therefore these matrices have a very similar structure. If the projection data vector y is ordered in such a way that all measurements of projection image j are before projection image $j + 1$ and the spacing in time between two

objects entering the scanner is an integer number of time steps k, all matrices A_i can be constructed by adding zero padding around the matrix for one object A. This can be achieved by multiplying A with a shifting matrix T_i in the following form:

$$T_i = \begin{bmatrix} \mathbf{0}_{(i \times M_h \times M_v \times k) \times m} \\ I_{m \times m} \\ \mathbf{0}_{remaining} \end{bmatrix}. \tag{8}$$

The first and the last block are matrices consisting of zeros and the middle block is an $m \times m$ identity matrix. Multiplying A with T_i shifts it by $k \times i$ projection images, because every projection image contains $M_h \times M_v$ measurements (one for every detector pixel). $\mathbf{0}_{remaining}$ pads the result with zeros until the end of the sequence.

The combined matrix B then consists of blocks of A and for the rest zeros. In the example below three projections overlap, so every row in the matrix crosses three blocks of matrix A:

$$B x_c = \begin{bmatrix} \ddots & \vdots & \vdots & \vdots & \vdots \\ & A & & & \\ & & A & & \\ & & & A & \\ & & & & A \\ \vdots & \vdots & \vdots & \vdots & \ddots \end{bmatrix} \begin{bmatrix} \vdots \\ x_i \\ x_{i+1} \\ x_{i+2} \\ x_{i+3} \\ \vdots \end{bmatrix} = y_c$$

$$= \sum_i T_i A x_i. \tag{9}$$

Each block column $T_i A$ of B can be divided vertically into blocks with a height of $M_h \times M_v \times k$. The next block column $T_{i+1} A$ can be obtained from the current block column $T_i A$ by adding an extra block of zeros on top and discarding the last block. This means B is a (band) block Toeplitz matrix. Moreover, because matrix B for q objects is the sum of q blocks that are shifted versions of matrix A, there is an upper bound on the rank given by:

$$\text{Rank}(B) \leq q \times \text{Rank}(A). \tag{10}$$

This means that when A is underdetermined B is also underdetermined.

Equation 9 holds for all conveyor belt shapes, as long as all objects follow the same trajectory and the spacing in time between objects is constant. For example S-turns or 3D trajectories are also possible. Two suggestions are illustrated in Figure 2.
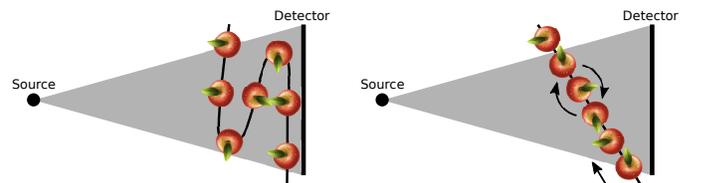
Fig. 2. Suggestions for TOP-CT scanning geometries.

III. RECONSTRUCTION METHODS

In this section several methods to making reconstructions from overlapping projection data are described. The first method solves the inverse to the full forward problem, so a reconstruction of all objects is found in one go by applying this method. The other methods are approximation methods that can be used to reconstruct objects one by one as they exit the scanner. Each method is given a name, which will be used in the results section. A small example problem is used to illustrate the steps of each method. This problem consists of a conveyor belt with 4 objects and a scanner where 2 objects have overlapping projections.

A. Similarities with reconstruction methods for non-overlapping data

The forward problems for CT imaging of a single object (Eq. 3) and of multiple objects with overlapping projections (Eq. 6) are very similar. Both are underdetermined linear forward problems affected by the same type of noise. Therefore the reconstruction methods for these problems are similar as well.

Because of the large size of both the projection data and the reconstruction data A may be too large to store in memory. However elements of A can be calculated on-the-fly whenever a vector matrix multiplication with A or A^T needs to be calculated [10]. Matrix vector multiplications with B or B^T can be written as sums of matrix vector multiplications with A, A^T, T_i and T_i^T, which can all be calculated on-the-fly. Therefore matrix vector multiplications with B or B^T can also be performed without needing the whole matrix B to be stored in memory.

The Simultaneous Iterative Reconstruction Technique (SIRT) [5] can be used to reconstruct a volume using this on-the-fly representation of the projection matrix. Other iterative methods could be used as well. Matrix B has structure that can potentially be used to solve the inverse problem in a more computationally efficient way. To highlight this structure for future research, the normal equations are written out in block matrix form for every method in this section.

B. Reconstructing all objects together (together)

When all projection data is available for a finite stream of objects, an inverse problem can be formulated using the full forward problem. For the example with 4 objects the full forward problem would be:

$$Bx_c = \begin{bmatrix} A & & & \\ & A & & \\ & & A & \\ & & & A \end{bmatrix} \begin{bmatrix} x_0 \\ x_1 \\ x_2 \\ x_3 \end{bmatrix} = y_c \quad (11)$$

$$= T_0 A x_0 + T_1 A x_1 + T_2 A x_2 + T_3 A x_3.$$

In this case SIRT can be applied directly on the projection data.

Algorithm 1 Reconstruct objects using the *together* method

1: $x_c \leftarrow \text{SIRT}(B, y_c)$

The normal equations for this problem are:

$$B^T B x_c = B^T y_c \text{ with } B^T B = \quad (12)$$

$$\begin{bmatrix} A^T A & A^T V_1 A & 0 & 0 \\ A^T V_{-1} A & A^T A & A^T V_1 A & 0 \\ 0 & A^T V_{-1} A & A^T A & A^T V_1 A \\ 0 & 0 & A^T V_{-1} A & A^T A \end{bmatrix}$$

$$\text{and } B^T = \begin{bmatrix} A^T & & & \\ & A^T & & \\ & & A^T & \\ & & & A^T \end{bmatrix} = \begin{bmatrix} A^T T_0^T \\ A^T T_1^T \\ A^T T_2^T \\ A^T T_3^T \end{bmatrix}.$$

Within $B^T B$ there are blocks $A^T T_i^T T_j A$. On the main diagonal $i = j$ and $T_i^T T_i = I$, so those blocks are $A^T A$. Moving away from the main diagonal $T_i^T T_j = V_{j-i}$, which is only determined by the difference between i and j. When $|j - i|$ is larger or equal to the maximum number of objects in view then $V_{j-i} = 0$ and otherwise $\text{Rank}(V_{j-i}) \leq M_h \times M_v \times (M_t - (|j - i| * k)))$, so the rank of the blocks is decreasing with their distance to the main diagonal. Moreover $V_j^T = V_{-j}$.

The $B^T B$ matrix has a band block Toeplitz structure, and is by construction positive semi-definite. This remains true for different stream lengths or numbers of objects whose projections are overlapping. The width of the band depends on the number of objects with overlapping projections, with blocks ranging from $A^T V_{-(p-1)} A$ to $A^T V_{p-1} A$ for p objects with overlapping projections.

Because the *together* method requires the projection data of all objects with overlapping projections it can not start as long as new objects with overlapping projections are being scanned. This makes the *together* method infeasible for the long streams of objects expected in an industrial setting, but it is useful as a baseline to compare the other methods to.

C. Reconstruct one object and ignore the overlap (ignore)

To reconstruct object x_i as soon as it exits the scanner a crude approximation to the forward problem of Equation 11 would be to approximate B with $T_i A$ and treat the overlapping projections as noise. This results in the following forward problem:

$$T_i A x_i \approx y_c, \quad (13)$$

and after multiplying both sides with T_i^T:

$$A x_i \approx T_i^T y_c. \quad (14)$$

Therefore, any existing reconstruction method that is available for the geometry of A can be used after doing this approximation. However, results are likely to contain errors because of the missing $T_j A x_j (j \neq i)$ terms.

Algorithm 2 Reconstruct objects using the *ignore* method

1: **for all** objects i **do**
2:      $x_i \leftarrow \text{SIRT}(A, T_i^T y_c)$
3: **end for**

The normal equations for this approximation are:

$$A^T A x_i = A^T T_i^T y_c. \quad (15)$$

D. Reconstruct one object by taking a submatrix of matrix B (submatrix)

A more accurate approximation of the forward problem for reconstructing object x_i is to take a horizontal slice of matrix B where x_i is included:

$$B_{sm}x_{sm\_i} = \begin{bmatrix} \boxed{A} & & \\ & \boxed{A} & \\ & & \boxed{A} \end{bmatrix} \begin{bmatrix} x_{i-1} \\ x_i \\ x_{i+1} \end{bmatrix} = T_i^T y_c \quad (16)$$

$$= V_{-1}Ax_{i-1} + Ax_i + V_1 Ax_{i+1}.$$

In contrast to Equation 13 this equation holds exactly, because it is a part of the full matrix B. SIRT can still be used to iteratively find a solution to Equation 16. For x_{i-1} and x_{i+1} not all available projection data is used, which results in limited angle artefacts. Because of this only the result for x_i is used and the rest of x_{sm_i} is discarded. The result for x_i is also slightly different as when it would have been calculated using the *together* method.

Algorithm 3 Reconstruct objects using the *submatrix* method

1: **for all** objects i **do**
2: $\quad x_{sm} \leftarrow \text{SIRT}(B_{sm}, T_i^T y_c)$
3: $\quad x_i \leftarrow \text{middle\_subvector}(x_{sm})$
4: **end for**

The normal equations for this problem are:

$$B_{sm}^T B_{sm} x_{sm\_i} = B_{sm}^T T_i^T y_c \text{ with } B_{sm}^T B_{sm} = \quad (17)$$

$$\begin{bmatrix} A^T V_{-1}^T V_{-1}A & A^T V_1 A & 0 \\ A^T V_{-1}A & A^T A & A^T V_1 A \\ 0 & A^T V_{-1}A & A^T V_1^T V_1 A \end{bmatrix}$$

$$\text{and } B_{sm}^T = \begin{bmatrix} \boxed{A^T} & & \\ & \boxed{A^T} & \\ & & \boxed{A^T} \end{bmatrix} = \begin{bmatrix} A^T V_{-1}^T \\ A^T \\ A^T V_1^T \end{bmatrix}.$$

E. Subtract already reconstructed objects from the projection data (subtract)

When reconstructing all objects on a conveyor belt using the *submatrix* method, each volume will be reconstructed multiple times. In the running example each object would be reconstructed three times, because the projections of each object overlap with two other objects, and this would be more in scanning geometries where the projections of more objects overlap. One approach to reduce the amount of double reconstruction work would be to backproject each reconstruction and subtract that from the projection data y_c. This removes the projection data of each object after it has been reconstructed so each object can be assumed to be the first of a stream, resulting in the following forward problem:

$$B_{st}x_{st\_i} = \begin{bmatrix} \boxed{A} & \\ & \boxed{A} \end{bmatrix} \begin{bmatrix} x_i \\ x_{i+1} \end{bmatrix} = T_i^T y_{s\_i} \quad (18)$$

$$= Ax_i + V_1 Ax_{i+1}.$$

Each subproblem can again be solved using SIRT, resulting in the following algorithm:

Algorithm 4 Reconstruct objects using the *subtract* method

1: $y_{st\_0} \leftarrow y_c$
2: **for all** objects i **do**
3: $\quad x_{st} \leftarrow \text{SIRT}(B_{st}, T_i^T y_{st\_i})$
4: $\quad x_i \leftarrow \text{top\_subvector}(x_{st})$
5: $\quad y_{st\_i+1} \leftarrow y_{st\_i} - T_i Ax_i$
6: **end for**

The normal equations for this problem are:

$$B_{st}^T B_{st} x_{st\_i} = B_{sts}^T T_i^T y_c \text{ with } B_{st}^T B_{st} = \quad (19)$$

$$\begin{bmatrix} A^T A & A^T V_1 A \\ A^T V_{-1} A & A^T V_1^T V_1 A \end{bmatrix}$$

$$\text{and } B_{st}^T = \begin{bmatrix} \boxed{A^T} & \\ & \boxed{A^T} \end{bmatrix} = \begin{bmatrix} A^T \\ A^T V_1^T \end{bmatrix}.$$

F. Runtime

In all methods presented in this section most of the computational work is done when calling SIRT. Within SIRT the most computationally expensive steps are performing the forward and backward projections. Therefore the runtime of the different methods is compared by looking at the number of forward and backward projection pairs that have to be performed. In the non overlapping case, performing t iterations of SIRT results in t forward and backward projections. When using the *ignore* method, SIRT is called in the same way, so t forward and backward projections are also performed per object. In the *together* method adding one object to the stream to be reconstructed would also result in t extra forward and backward projections. In the *submatrix* and *subtract* methods the number of forward and backward projections depend on the number of objects p that are visible on the detector at the same time. In the *submatrix* method $2p - 1$ objects are being reconstructed, but except for the middle object all objects are only visible in some of the projection images. Because each projection image includes at most p objects, t iterations of SIRT can be performed using a number of calculations equivalent to at most tp full forward and backward projections. In the *subtract* method objects are gradually being added. In the first $\frac{1}{p}$ of the projections one object is visible. In the second $\frac{1}{p}$ of the projections two objects are visible etc. This results in $\sum_{i=0}^{p} \frac{i}{p} = \frac{p+1}{2}$ objects being visible on average so the runtime is equivalent to $t\frac{p+1}{2}$ full forward and backward projections. An overview of the number of projections of the presented methods is presented in Table I.

TABLE I
FORWARD AND BACKWARD PROJECTIONS WHEN DOING t ITERATIONS OF SIRT WITH AT MOST p OBJECTS VISIBLE ON THE DETECTOR

Method	Full forward and backward projections per reconstructed object
SIRT without overlap	t
Together (per object)	t
Ignore	t
Submatrix	tp
Subtract	$t\frac{p+1}{2}$

IV. Experiments

To compare the proposed methods and to study the effect of overlapping projections, three experiments have been performed. The first two experiments use simulated data, and were performed to compare the image quality between the different methods, and between overlapping and non-overlapping projection data, measured by the peak signal to noise ratio (PSNR) and the structural similarity index metric (SSIM) [27]. In addition, the methods have been tested on a real data-set to verify the problem formulation and to test the robustness to realistic noise.

A. Reconstruction strategies with overlapping projections

The goal of this experiment was to compare the reconstruction quality of the reconstruction methods introduced in Section III, and to see how the one by one methods perform in comparison to the *together* method. An overlapping projection dataset was simulated which was used as the input for each method. Because the projection data was simulated, the input volumes to the simulation could be used as a ground truth to calculate performance metrics for all the reconstructed volumes.

A dataset of CT reconstructions of apples was used as the input to the simulations. A different subset of this dataset has been shared before [2]. Apples naturally contain variations in shape and size, features at different scales and both hard edges and smooth transitions, making this a suitable benchmark dataset. The dataset was preprocessed so that a mask of each apple was available and each mask would fit within a cylinder with a diameter of 256 voxels and a height of 237 voxels. For this experiment projection data from 68 apples was simulated with a scanning geometry where the apples would move in a U-turn between a fixed source and detector. On the curved section of the U-turn the apples would rotate uniformly along with the curve. This geometry is slightly incomplete in similar ways as the circular cone beam geometry [6] so it does not satisfy the Tuy-Smith condition [25, 23]. The geometry is illustrated in Figure 3. Each apple would be visible for 400 projections and a new apple would enter the field of view of the setup every 48 projections. Because of this at most 9 apples were visible in each projection image. The projection images are 512×1030 pixels. Poisson noise was added to the projection data with a photon count of 25000 photons. The attenuation coefficient of all apples was divided by a factor $2^{1.5}$ based on the results of the second experiment.

This dataset was used as the input to the four reconstruction methods introduced in section III. SIRT was used with a non-negativity constraint and a cylindrical reconstruction mask. The optimal number of SIRT iterations was determined every time when SIRT was executed by comparing the reconstructions with the original volumes from the apple dataset using the PSNR inside the mask of the apple. SIRT was stopped if the PSNR of a reconstruction after a SIRT iteration was worse than the previous PSNR for 30 consecutive iterations. While comparing to a ground truth is not possible in practice it makes sure that the number of SIRT iterations is tuned in the same way for the different methods, so they can be compared
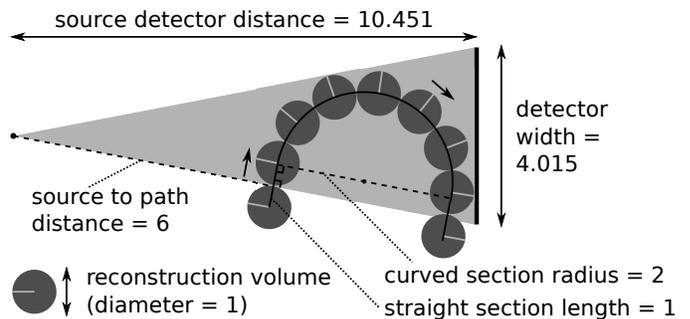
Fig. 3. Illustration of the scanning geometry used in the first experiment. Each circle represents the reconstruction volume of one object, and at most 9 objects can be in view at a given time. Each object moves $\frac{1}{400}$th of the trajectory between two projections, so for each object 400 projections are made and after that they leave the scanning setup. Every 48 projections a new object starts on the left end of the trajectory.

in a fair way. Moreover, the *ignore* method was also tested at a fixed number of 100 iterations, because according to the PSNR the optimal number would be only one iteration.

For every reconstruction the PSNR and SSIM over vertical slices were calculated. The metrics from first and last 9 apples were discarded because the projections of these apples were not fully overlapping, so 50 apples were included in this experiment. The results are presented in Table II and Figure 4.

Method	PSNR	Mean SSIM	Iterations
Together	33.48($\pm$0.17)	0.830($\pm$0.005)	551
Submatrix	33.56($\pm$0.17)	0.832($\pm$0.004)	611($\pm$28.7)
Subtract	32.59($\pm$0.20)	0.808($\pm$0.006)	318($\pm$15.5)
Ignore (1 it.)	19.15($\pm$0.57)	0.745($\pm$0.012)	1
Ignore (100 it.)	17.40($\pm$0.47)	0.722($\pm$0.012)	100

The *together*, *submatrix* and *subtract* methods performed very similarly, both in the metrics as in the appearance of the reconstructions. The *submatrix* method performed best overall, but the performance increase compared to the *together* method could be caused by the way the number of iterations was tuned: In the *submatrix* method the number of SIRT iterations was tuned per object, while only one number of iterations could be tuned in the *together* method. The *ignore* method doesn't take into account the other volumes and because of this the reconstructions have higher values. These artefacts had a big impact on the PSNR scores, causing the optimal iterations to be only 1 according to the PSNR. However, when doing 100 iterations many details can be recognized in the reconstructions. Despite the fact that the geometry does not satisfy the Tuy-Smith condition no cone beam artifacts or missing angle artifacts were observed in the reconstructions.

Because the *subtract* method uses the previous reconstructions, it could be possible that an error would accumulate resulting in a lower reconstruction quality over time. A similar effect might also occur in the *together* method with reconstructions close to either end of the stream potentially performing better. To test how much the reconstruction quality of these

Together

Submatrix

Subtract

Ignore (1 SIRT iteration)

Ignore (100 SIRT iterations)

Input data
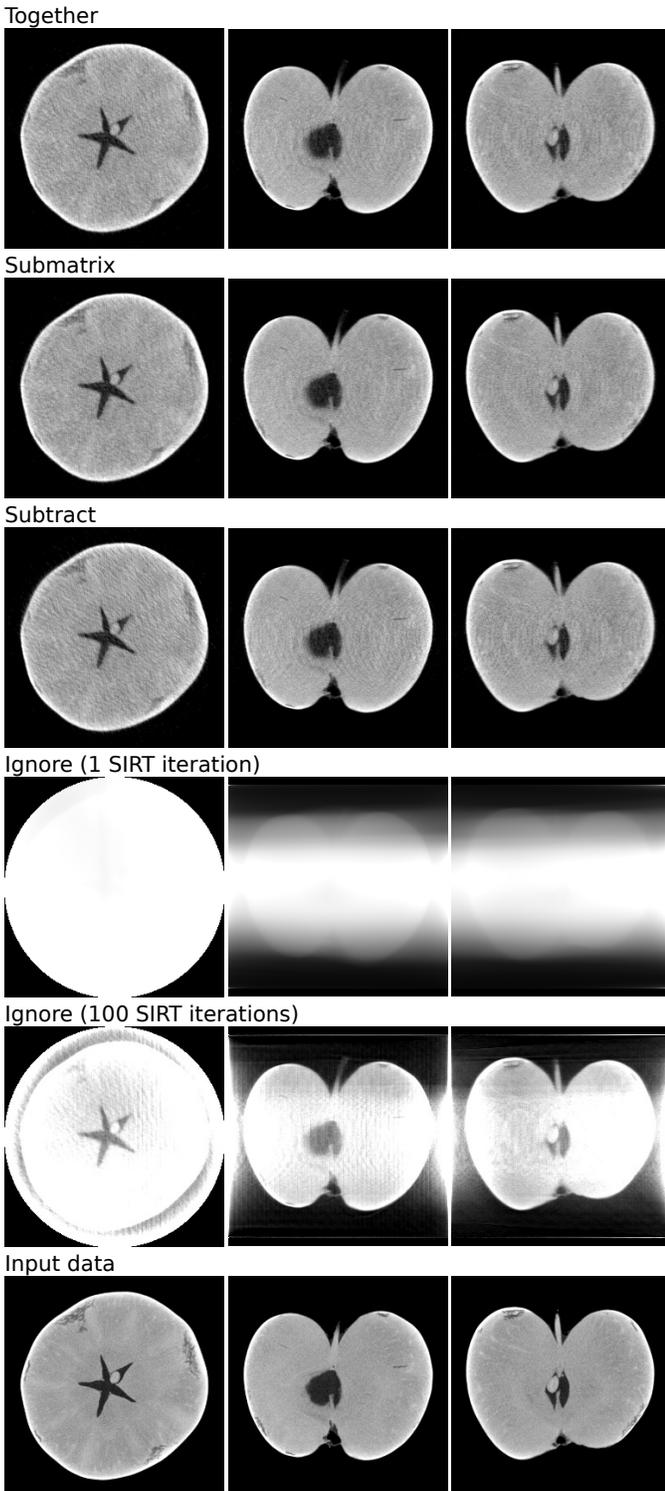
Fig. 4. Comparison of reconstructions made with different strategies for handling overlapping projection data. For every reconstruction method 3 orthogonal slices through the middle of the 32nd apple of the stream are displayed. The same color map was used on all images in this figure for easier comparison.

methods changes over time both methods were compared over time with the *submatrix* method, which can not accumulate error over time because it uses only local projection data. The PSNR over time is plotted in Figure 5. In that figure

no time related performance changes could be observed on both methods.
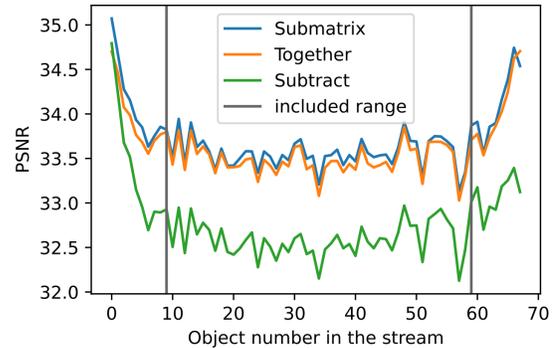
Fig. 5. PSNR over time using the *submatrix*, *together* and *subtract* methods. The *submatrix* method can not have time related performance changes, and by comparing the *together* and *subtract* methods to this method no time related PSNR changes could be observed.

B. Overlapping and non-overlapping projection data

The goal of this experiment was to gain insight in the effect of overlapping projections on reconstruction quality. To investigate this, reconstructions were compared that were made from equal amounts of total projection data over a stream of objects with and without overlapping projections.

The attenuation coefficient within an object depends on the voltage supplied to the X-ray source. The source voltage is commonly tuned so that the projection data uses the full dynamic range of the detector. When X-rays pass through multiple objects they get attenuated within each object, resulting in lower detector measurements in areas where the projections of multiple objects overlap. Because of this the optimal tube voltage for an overlapping setup is different than for a non-overlapping setup. In this experiment the process of tuning the tube voltage is approximated by multiplying the attenuation coefficient in all voxels by a single value. This makes it possible to compare overlapping and non-overlapping geometries at their optimal range of detector values on the same set of input objects.

The same apple dataset as in the previous experiment was used to generate simulated projection data. Two sets of projection datasets were simulated from the first 38 apples in the apple dataset, one with overlapping projections and one with no overlap. For the overlapping projections the same scanning setup was used as in the previous experiment (Figure 3). For the non-overlapping projections the setup was modified. Instead of moving $\frac{1}{400}$th of the trajectory between two projections, each apple would move $\frac{1}{48}$th of the trajectory. A new apple would still be added every 48 projections, so only one apple would be in view in every projection image. This resulted in fewer projections per apple, but the same number of total projections over all apples. Again Poisson noise was simulated with 25000 photons. 15 different versions of each dataset were made, where the attenuation coefficient of all apples was multiplied before projecting them. The attenuation multipliers were taken over an exponential range between 2^{-5} and 2^2 with a multiplicative step size of $\sqrt{2}$.

Reconstructions were made of each apple from both the overlapping and non-overlapping projections for every attenuation multiplier. Like in the previous experiment the first and the last 9 reconstructions were discarded in every stream because their projections were not fully overlapping and the remaining 20 reconstructions were compared based on the PSNR and SSIM. For the overlapping dataset the *together* method was used and for the non-overlapping dataset SIRT was used without modifications. For all reconstructions SIRT had the same settings as in the previous experiment, so it used a non-negativity constraint, cylindrical reconstruction volumes, and the number of iterations was selected to be optimal according to the PSNR. How the PSNR and SSIM vary over the attenuation coefficient multiplier is plotted in Figure 6. An example of a reconstruction at the optimal attenuation multiplier of both setups is shown in Figure 7.
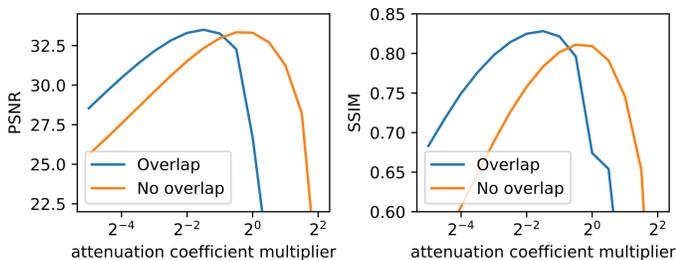
Fig. 6. Comparison of reconstruction quality between two similar setups, one with and one without overlapping projections. The attenuation coefficients of the objects were multiplied over a range of values before simulating noisy projections and making reconstructions.
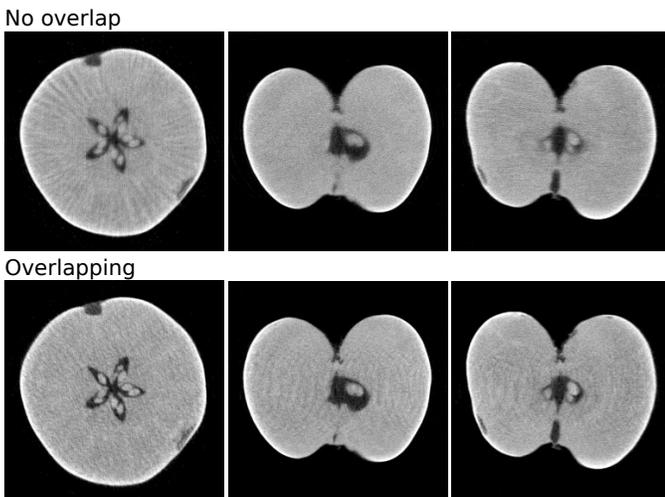
Fig. 7. Comparison of reconstructions made from overlapping projection data to reconstructions from non-overlapping projection data. For both datasets 3 orthogonal slices through the middle of the 19th apple are displayed. The same color map was used on all images in this figure for easier comparison.

As expected, the optimal reconstruction results are achieved at a lower attenuation coefficient for the setup with overlap than for the setup without overlap. The PSNR at the optimum of both methods is almost the same (overlap: 33.50, no overlap: 33.34), while the mean SSIM is higher for the reconstructions from the overlapping setup (overlap: 0.828, no overlap: 0.811). Visually the reconstructions from the

overlapping setup appear sharper which could be caused by the fact that projection data from more angles is available in the overlapping case. The reconstructions from the overlapping setup also show repeating artifacts.

C. Real life dataset of overlapping mandarin projections

The goal of this experiment was to test if the methods from Section III would also work on real life data. A scanning geometry similar to a conveyor belt could be set up in a lab scanner by using a few additional components and a custom scanning protocol. The methods from Section III were applied to the dataset acquired using this setup and the results were compared visually.

A dataset of 23 mandarins was acquired in the FleX-ray scanner at the CWI in Amsterdam [22]. This scanner does not have a conveyor belt to move multiple samples at the same time. Therefore we developed a method to acquire data similar to a conveyor belt scanning setup without extensively modifying the scanner. A wooden disk was attached on top of the rotation stage and six evenly spaced object positions were marked on the disk at a fixed distance from the center of rotation. Pieces of cardboard tube were used as sample holders to make sure the mandarins wouldn't roll as the disk would rotate and to raise them from the disk without attenuating too much of the X-ray signal. The rotation stage was positioned in such a way that over a full rotation of the disk, each mandarin would be completely in view of the detector for more than 180 degrees of the rotation, while there would also be a position at which it would be completely out of view. Figure 8 illustrates the whole geometry and Figure 9 shows a picture of the mandarins on the disk.
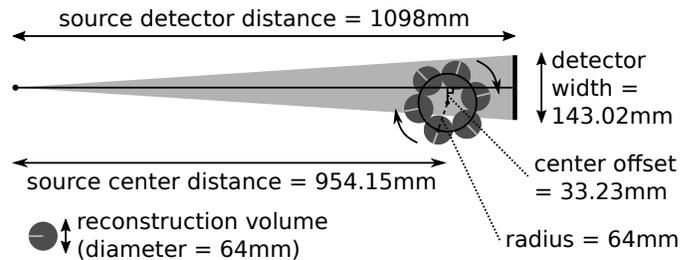
Fig. 8. Illustration of the scanning geometry used in the real life experiment. Each object moves $\frac{1}{2400}$ of the circular trajectory between two projections. After moving over the full circle each object is replaced with a new object while it is out of view of the scanning setup.

The scan was performed in phases. Every phase 400 projection images were acquired, while rotating the disk for 60 degrees. This would rotate one of the positions out of view of the scanning setup. Before the first 6 phases a mandarin was added on the position that was out of view of the setup. For the phases after that the position that would be out of view would contain a mandarin that had rotated the full circle so that mandarin was replaced with a new mandarin. At the last 6 phases there would be no new mandarins left to add so the mandarin that was out of view of the setup would only be removed. The projection images acquired from each phase were concatenated resulting in a dataset of 11200 projections of 956x500 pixels. At most 5 mandarins were in view at a
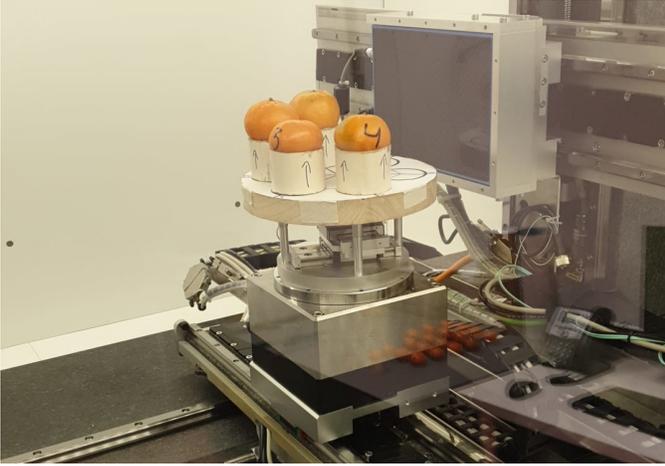
Fig. 9. Picture of the setup used for the acquisition of the mandarin dataset. The first four mandarins have been placed on the rotating disk in front of the detector.

given time. The X-ray tube was set to a peak voltage of 90kV and a target power of 49.5W. Moreover, the exposure time was 200ms and 0.1mm of copper was used to filter the source spectrum. An example of a projection image is given in Figure 10.
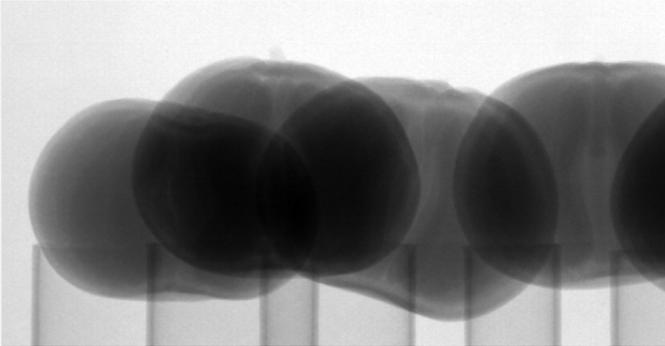
Fig. 10. Example projection image from the real life dataset of overlapping mandarin projections.

Reconstructions were made from this dataset with the *together*, *submatrix* and *subtract* methods using 100 iterations of SIRT with a non-negativity constraint. An example of a reconstruction of each method is shown in Figure 11.

Like in the simulation experiment, the results from the *together* and *submatrix* methods are almost identical. Some unsharpness and artifacts can be observed in the reconstructions of both methods. We expect that this was caused by a mismatch between the geometry that was used in the reconstruction algorithm and the real geometry. A manual adjustment to the center offset parameter (Fig. 9) already reduced these errors and we expect further improvements are possible by fully calibrating the geometry. The *subtract* method appears to be more sensitive to calibration errors as the reconstructions made with this method contain a lot more artifacts in this experiment.

Together

Submatrix

Subtract
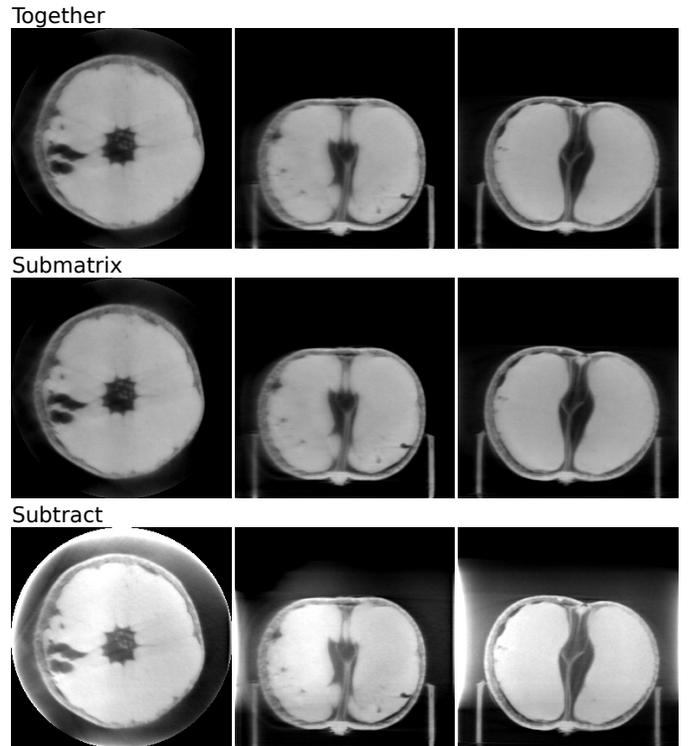
Fig. 11. Orthogonal slices of the reconstruction of the thirteenth mandarin from the real life dataset of overlapping mandarin projections. The same color map was used on all images in this figure for easier comparison.

D. Implementation and dataset

The code for all experiments is available on Github [21] and the mandarin dataset is available on Zenodo [22].

To represent matrix A the `Operator` class from the Tomosipo library [10] was used. To represent matrix B and it's variants a `MultiOperator` class was implemented that had mostly the same interface as a Tomosipo `Operator`. This made it possible to use the same implementation of SIRT for both A and B.

V. DISCUSSION

By allowing overlapping projections, an extra degree of freedom is added to the design space of industrial CT scanners. Future research could be aimed at speeding up the reconstruction process and finding the optimal designs for different practical applications.

Firstly, the computation time required to make 3D reconstructions with SIRT might be too long for real time applications. Replacing SIRT with Nesterov accelerated gradient descent [17] might result in fewer iterations being required. Another direction for developing faster reconstruction algorithms would be to look for a fast approximation to the effects of overlap. The fact that the *ignore* method already produced visually recognizable results while completely ignoring the overlap suggests that this might be possible. The *ignore* method itself might be sped up by employing an (approximate) backprojection type reconstruction algorithm instead of SIRT. Moreover, deep learning could be used to speed up the reconstruction by replacing the iterative algorithm with fewer

iterations in an unrolled iterative scheme or by reducing the artifacts from the *ignore* method. Alternatively, applications where acquisition time is expensive, but computation time is abundantly available could be investigated, such as scanning objects in a synchrotron.

Secondly, more advanced reconstruction methods could be used that make use of more prior information to get better reconstruction results using the same projection data. Currently only a non-negativity constraint and early stopping are used as regularization, but results could be improved by adding additional regularization such as Total Variation(TV) [14], or by adding a neural network as a post-process. Given that on many conveyor belts the objects are very similar, neural networks for improving the reconstruction quality can be trained to use domain knowledge of the specific type of object on the conveyor belt.

Thirdly, when designing a scanner a trade-off needs to be made between the throughput, reconstruction quality and cost of the setup, which is highly application dependent. All geometries used in this paper consist of a U-turn movement. However, the same formulations can be used to represent different geometries as well. Optimization algorithms could be used to find optimal geometries similarly to how robot arm CT geometries are optimized [11]. Apart from the geometry the trade-off between other parameters could be further investigated and optimized such as: the number of overlapping objects, the number of projections, detector size, tube current, tube voltage and exposure time.

VI. CONCLUSION

A new class of geometries for high throughput industrial CT scanning called TOP-CT was investigated. The main conclusions are: TOP-CT can be formulated as a linear forward problem with a band block Toeplitz structure (Section II). The inverse of this forward problem can be solved completely or object by object using existing iterative methods such as SIRT, requiring only a small modification to existing software toolkits (Section III). For a U-turn geometry objects can be reconstructed as soon as they exit the scanner using the *submatrix* method without loss of reconstruction quality compared to the baseline *together* method (Section IV). With overlapping projection data a similar (PSNR) or slightly better (SSIM) reconstruction quality can be achieved as with non-overlapping projection data acquired over the same time. To get the best results with overlapping projection data the attenuation of the objects should be lower than with non-overlapping projection data, which may be achieved by changing the source voltage (Section IV). This new approach to CT scanning can simplify the mechanical design of high throughput industrial CT scanners and reduce the detector size, which may help realize the vision of industry 4.0.

ACKNOWLEDGEMENTS

REFERENCES

[1] Marcin B Bauza, Jason Tenboer, Ming Li, Aleksandr Lisovich, Jian Zhou, Daniel Pratt, Jonathan Edwards, Hai Zhang, Charles Turch, and Richard Knebel. Realization of industry 4.0 with high speed ct in high volume production. *CIRP Journal of Manufacturing Science and Technology*, 22:121–125, 2018.

[2] Sophia Bethany Coban, Vladyslav Andriiashen, Poulami Somanya Ganguly, Maureen van Eijnatten, and Kees Joost Batenburg. Parallel-beam x-ray ct datasets of apples with internal defects and label balancing for machine learning. *arXiv preprint arXiv:2012.13346*, 2020.

[3] Leonardo De Chiffre, Simone Carmignato, J-P Kruth, Robert Schmitt, and Albert Weckenmann. Industrial applications of computed tomography. *CIRP annals*, 63(2):655–677, 2014.

[4] Thomas De Schryver, Jelle Dhaene, Manuel Dierick, Matthieu N Boone, Eline Janssens, Jan Sijbers, Mattias van Dael, Pieter Verboven, Bart Nicolai, and Luc Van Hoorebeke. In-line ndt with x-ray ct combining sample rotation and translation. *NDT & E International*, 84:89–98, 2016.

[5] Tommy Elfving, Per Christian Hansen, and Touraj Nikazad. Semiconvergence and relaxation parameters for projected sirt algorithms. *SIAM Journal on Scientific Computing*, 34(4):A2000–A2017, 2012.

[6] Lee A Feldkamp, Lloyd C Davis, and James W Kress. Practical cone-beam algorithm. *Josa a*, 1(6):612–619, 1984.

[7] Federico Giudiceandrea, Alexander Katsevich, and E Ursela. A reconstruction algorithm is a key enabling technology for a new ultrafast ct scanner. *SIAM News*, 49:1–11, 2016.

[8] Federico Giudiceandrea, Enrico Ursella, and Enrico Vicario. A high speed ct scanner for the sawmill industry. In *Proceedings of the 17th international non destructive testing and evaluation of wood symposium*, pages 14–16, 2011.

[9] Per Christian Hansen, Jakob Jørgensen, and William RB Lionheart. *Computed Tomography: Algorithms, Insight, and Just Enough Theory*. SIAM, 2021.

[10] Allard Hendriksen, Dirk Schut, Willem Jan Palenstijn, Nicola Viganò, Jisoo Kim, Daniël Pelt, Tristan van Leeuwen, and K. Joost Batenburg. Tomosipo: Fast, flexible, and convenient 3D tomography for complex scanning geometries in Python. *Optics Express*, 2021.

[11] Gabriel Herl, Jochen Hiller, Mareike Thies, Jan-Nico Zaech, Mathias Unberath, and Andreas Maier. Task-specific trajectory optimisation for twin-robotic x-ray tomography. *IEEE Transactions on Computational Imaging*, 7:894–907, 2021.

[12] Eline Janssens, Jan De Beenhouwer, Mattias Van Dael, Thomas De Schryver, Luc Van Hoorebeke, Pieter Verboven, Bart Nicolai, and Jan Sijbers. Neural network hilbert transform based filtered backprojection for fast inline x-ray inspection. *Measurement Science and Tech-*

nology, 29(3):034012, 2018.

[13] Baodong Liu, James Bennett, Ge Wang, Bruno De Man, Kai Zeng, Zhye Yin, Paul Fitzgerald, and Hengyong Yu. Completeness map evaluation demonstrated with candidate next-generation cardiac ct architectures. *Medical physics*, 39(5):2405–2416, 2012.

[14] Yang Lu, Zhenyu Yang, Jun Zhao, and Ge Wang. Tv-based image reconstruction of multiple objects in a fixed source-detector geometry. *Journal of X-ray Science and Technology*, 20(3):277–289, 2012.

[15] Andreas Maier, Patrick Kugler, Günter Lauritsch, and Joachim Hornegger. Discrete estimation of data completeness for 3d scan trajectories with detector offset. In *Bildverarbeitung für die Medizin 2015*, pages 47–52. Springer, 2015.

[16] Ed Morton, Ken Mann, Ari Berman, Michael Knaup, and Marc Kachelrieß. Ultrafast 3d reconstruction for x-ray real-time tomography (rtt). In *2009 IEEE Nuclear Science Symposium Conference Record (NSS/MIC)*, pages 4077–4080. IEEE, 2009.

[17] Yurii Nesterov. *Introductory lectures on convex optimization: A basic course*, volume 87. Springer Science & Business Media, 2003.

[18] Neil S O'Brien, Richard P Boardman, Ian Sinclair, and Thomas Blumensath. Recent advances in x-ray cone-beam computed laminography. *Journal of X-ray science and technology*, 24(5):691–707, 2016.

[19] Luis F Alves Pereira, Eline Janssens, George DC Cavalcanti, Ren Tsang, Mattias Van Dael, Pieter Verboven, Bart Nicolai, and Jan Sijbers. Inline discrete tomography system: Application to agricultural product inspection. *Computers and electronics in agriculture*, 138:117–126, 2017.

[20] Letitia Schoeman, Paul Williams, Anton du Plessis, and Marena Manley. X-ray micro-computed tomography (μct) for non-destructive characterisation of food microstructure. *Trends in Food Science & Technology*, 47:10–24, 2016.

[21] Dirk Elias Schut. top-ct_experiments github repository. https://github.com/D1rk123/top-ct_experiments, 2022.

[22] Dirk Elias Schut. Trajectory with Overlapping Projections x-ray Computed Tomography (TOP-CT) dataset of 23 mandarins moving over a circular trajectory. https://doi.org/10.5281/zenodo.6351647, 2022.

[23] Bruce D Smith. Image reconstruction from cone-beam projections: necessary and sufficient conditions and reconstruction methods. *IEEE transactions on medical imaging*, 4(1):14–25, 1985.

[24] Adam Thompson, Ian Maskery, and Richard K Leach. X-ray computed tomography for additive manufacturing: a review. *Measurement Science and Technology*, 27(7):072001, 2016.

[25] Heang K Tuy. An inversion formula for cone-beam reconstruction. *SIAM Journal on Applied Mathematics*, 43(3):546–552, 1983.

[26] Enrico Ursella, Federico Giudiceandrea, and Marco Boschetti. A fast and continuous ct scanner for the optimization of logs in a sawmill. In *8th Conference on Industrial Computed Tomography (iCT 2018) at Wels, Austria*, volume 2, 2018.

[27] Zhou Wang, Alan C Bovik, Hamid R Sheikh, and Eero P Simoncelli. Image quality assessment: from error visibility to structural similarity. *IEEE transactions on image processing*, 13(4):600–612, 2004.

[28] Bruce R Whiting, Parinaz Massoumzadeh, Orville A Earl, Joseph A O'Sullivan, Donald L Snyder, and Jeffrey F Williamson. Properties of preprocessed sinogram data in x-ray computed tomography. *Medical physics*, 33(9):3290–3303, 2006.

Dirk Elias Schut received a Bsc. in Computer Science and a double Msc. in Computer Science and Electrical Engineering, both from Delft University of Technology. Currently he is working as a PhD researcher at the Computational Imaging group of the Centrum Wiskunde & Informatica (CWI) in the Netherlands. His research is part of the UTOPIA project on bringing per product CT imaging for quality control to food processing factories.

Kees Joost Batenburg is a professor at the Leiden Institute of Advanced Computer Science (LIACS) and his chair is Imaging and Visualization. He founded the FleX-Ray lab at the Centrum Wiskunde & Informatica (CWI), where a custom-designed CT system is linked to advanced data processing and reconstruction algorithms. He published more than 80 journal articles and more than 60 conference papers in the field of tomographic image processing and reconstruction.

Robert van Liere received the PhD degree in computer science from the University of Amsterdam. He is a principal investigator at the Computational Imaging group of the Centrum Wiskunde & Informatica (CWI) and a full professor at the Eindhoven University of Technology. His research interests include interactive visualization, virtual environments, and human-computer interaction.

Tristan van Leeuwen is the group leader of the Computational Imaging group at the Centrum Wiskunde & Informatica (CWI) in the Netherlands. He received his BSc. and MSc. in Computational Science from Utrecht University. He obtained his PhD. in geophysics at Delft University in 2010. After spending some time as a postdoctoral researcher at the University of British Columbia in Vancouver, Canada and the CWI, he returned to Utrecht University in 2014 as an assistant professor at the mathematical institute. In 2021, he moved to his current position. His research interests include: inverse problems, computational imaging, tomography and numerical optimization.